Design of minimal dispersion fluidic channels in a CAD-free framework

By B. Mohammadi† J. I. Molho‡ AND J. G. Santiago‡

We show the application of our shape optimization approach to the design of electroosmotic micro-fluidic channels realizing minimal geometrical dispersion on 90- and 180-degree turns.

1. Introduction

Microfluidic channel systems used in bio-analytical applications are fabricated using technologies derived from microelectronics industry including lithography, wet etching, and bonding of substrates. One important class of these channel system uses capillary zone electrophoresis to separate and detect chemical species. This technique separates chemical species suspended in a liquid buffer based on their electrophoretic mobility. The electric field in these systems is applied along the axis of the channel using electrodes immersed at reservoirs at the end of the micro-channels. The ability to discriminate between sample species of nearly equal mobility is enhanced by increasing the channel length (Culbeston, Jacobson & Ramsey (1998), Molho *et al.* (2000)). In order to achieve channel lengths of order 1 m and yet confine the micro-channel system to a compact configuration with dimensions less than about 10 cm, curved channel geometries are required. Unfortunately, curved channel geometries introduce skew, which creates a dispersion of the electrophoretic sample bands in the flow. This curved-channel dispersion has been identified as an important factor in the decrease of separation efficiency of electrophoretic micro-channel systems. The goal of the current work is to analyze and then minimize the skew that is introduced by turns in electrokinetic microchannels. Unfortunately, we notice that reducing the skew often introduces a new type of residual dispersion associated with band advection away from the channel boundaries. To avoid this effect it is necessary for the channel walls to be as smooth as possible with minimal curvature variation. However, optimizations based only on skew minimization do not yield smooth walls. We therefore add a constraint on the wall smoothness to our optimization.

The optimization formulation for such devices has to include therefore the following points:

- minimize the skew due to turns,
- minimize the residual dispersion associated with band advection,
- avoid too much variations in walls curvature,
- maximize the length of the channel,
- minimize the occupied surface.

Our aim in this paper is to show how to use our optimization platform, first designed

† University of Montpellier and INRIA, France
‡ Mechanical Engineering Dept., Stanford University, Stanford, CA, USA

for aeronautical applications (Mohammadi (1997a),Mohammmadi & Pironneau (2000)), for the design of minimal dispersion electrokinetic channels.

An important ingredient in the platform is the Computer-Aided-Design-free parameterization of the micro-fluidic channel geometry which has shown its ability to produce various new shapes not necessarily reachable in the original CAD parameterization. In this parameterization, the control space is quite rich compared to a CAD parameterization (Mohammmadi & Pironneau (2000)). We will see also that this parameterization allows for modeling of dimensional uncertainties introduced by the manufacturing step.

Another important ingredient is to use dynamic minimization algorithms. We showed how to put well known minimization algorithms in the form of dynamic systems, having a decreasing energy like in Hamilton-Jacobi systems, suitable to reach stationary point for the solution of coupled problems. Indeed, in this approach, the minimization algorithm is seen as an extra state equation (for the parameterization) and the whole system is marched in a pseudo-time to a stationary point. Global minimization can also be introduced by coupling several dynamic systems from different parameterization states (Mohammmadi & Pironneau (2000)).

Finally, we would like to point out the use of incomplete sensitivities in the design process. The aim is to perform analysis and design at the same time. The main idea is to use two different state equations for the evaluation of the state variables and for the evaluation of sensitivities. The first is usually complex and probably available in a commercial package; the second one simpler, but of which we have complete control and knowledge. The two different state equations are used because we would like the simulation and design problems to have about the same complexity. We widely used this technique in shape design in aerodynamical applications (Mohammmadi & Pironneau (2000)) where the gradient of aerodynamical coefficients were approximated keeping only geometrical contributions (Mohammadi (1997a),Mohammmadi & Pironneau (2000)). This is especially important where the number of control parameters is large and would otherwise require the use of an adjoint solver. This simplification is also important when the size of the direct simulation problem is near the limit of what can be treated in a reasonable amount of time by existing computer facilities.

We show the application of this technique by minimizing the dispersion of chemical species moving electrokinetically through 90 and 180 degree turns. These turns are important as they can be used to make serpentine channels that provide long separation lengths within a compact area. Typical cross-section sizes for these channels are 100 μm in width and 10 μm in depth.

2. Governing equations

This problem is multi-model in the sense that several PDE are involved in the definition of the state variables and the cost function. We will see that different levels of approximation can be introduced for these state equations.

2.1. *Electric field*

We desire to simulate the motion of species in an electric field $E(t, x)$. In general, E can be either stationary or unsteady, but in this work, we consider only steady electric fields.

$E = \nabla v$ is defined solving a Poisson equation for the potential v:

$$-\Delta v = 0, \quad \text{in } \Omega \tag{2.1}$$

$$v(\Gamma_{in}) = v_1, \quad v(\Gamma_{out}) = v_2, \quad \frac{\partial v}{\partial n} = 0 \quad \text{on other boundaries.}$$

2.2. *Flow motion*

For typical electrokinetic microchannel applications, the observed flow motion has a velocity of about $10^{-4}m/s - 10^{-3}m/s$, channel thickness of 100 μm, and kinematic viscosity about $10^{-5}m^2s^{-1}$. This leads to Reynolds numbers ranging from 0.001 to 0.01. Due to spontaneous charge separation that occurs at the channel walls, there is formation of an electric double layer (Probstein). The typical size of this layer is a few nano meters. The stiffness of this electric double layer makes it difficult to compute using classical numerical approaches applied to the Stokes model with a Lorentz force term. However, it is known that at the edge of the double layer the flow is parallel and directly proportional to the electric field. The first model describing the flow motion can therefore be the Stokes system with a slip velocity at the channel walls.

$$\frac{\partial U}{\partial t} - \mu \Delta U + \nabla p = 0, \quad \text{in the channel} \tag{2.2}$$

$$U = \mu_{ek} E \quad \text{on the inner and outer walls,}$$

$$-\mu \frac{\partial U}{\partial n} + p.n = 0 \quad \text{on in and outflow boundaries,}$$

where μ_{ek} is the electrokinetic mobility of the flow, μ the dynamic viscosity, and n the unit external normal to the boundaries.

2.3. *Reduced models for the flow*

In the absence of a pressure gradient, the previous model reduces to two elliptic equations for the velocity components and states that the velocity vector is locally parallel to the walls and proportional to the local electric field $U = \mu_{ek} E\tilde{U}$ with $\tilde{U}$ obtained solving for $\tilde{U} = (\tilde{u}_1, \tilde{u}_2)$:

$$-\Delta \tilde{u}_1 = 0, \quad -\Delta \tilde{u}_2 = 0, \quad \text{in} \quad \Omega, \tag{2.3}$$

$$\tilde{U} = (\tilde{u}_1, \tilde{u}_2) = \tau = (\tau_1, \tau_2), \quad \text{on channel walls,} \quad \frac{\partial \tilde{U}}{\partial n} = 0 \quad \text{on other boundaries,}$$

where τ is the local unit tangent to channel walls. Noticing that the electric field itself is parallel to walls, this means that the velocity is everywhere parallel and proportional to the electric field:

$$U = \mu_{ek} E. \tag{2.4}$$

We use this latter model in our optimization problem. In addition, this model is interesting for incomplete sensitivity evaluation (see below), where different models are used for the state and gradient computations. In other words, even when using more complex models, we should consider this model as the state equation to be used for sensitivity evaluation.

2.4. *Advection of species*

The motion of a species a at infinite Peclet number by the velocity field U computed above is described by:

$$a_t(x,t) + U(x)\nabla a = 0, \quad \text{in} \quad \Omega, \tag{2.5}$$

$$a(\Gamma_{inlet}) = \text{given.}$$

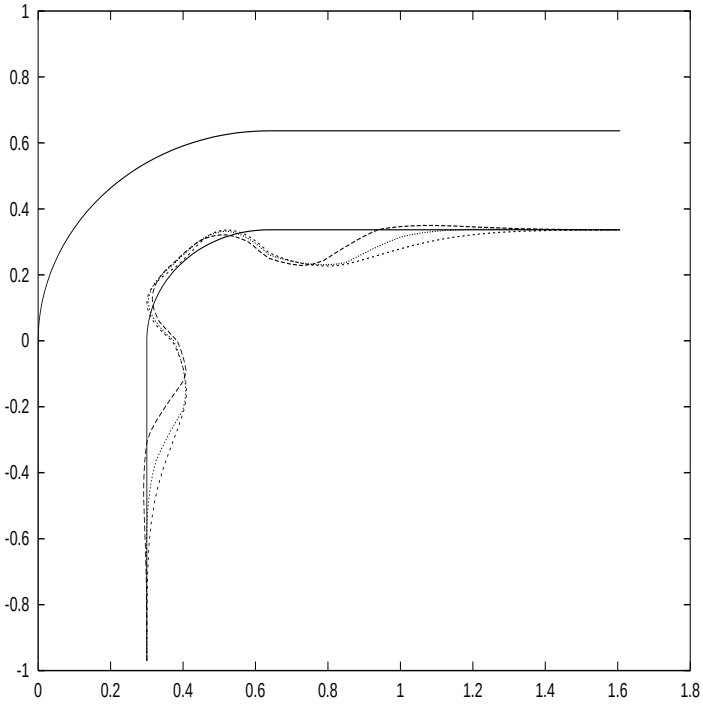

FIGURE 1. Shapes obtained under the same optimization conditions for three admissible spaces with different minimum required regularity for the shape. I: initial (———), II: less regular (— — —), III: medium regularity (- - - -), IV: most regular (·····).

As we consider the velocity field defined by the stationary electric field, this step is therefore only a post-processing step and is devoted to the quantification of the skew.

3. Design problem formulation

We consider the following constrained minimization problem:

$$\min_{x(t)\in X} J(x, q(x), u(q, x)), \tag{3.1}$$

$$E(x, q(x), u(q, x)) = 0,$$

$$g_1(x) \leq 0, g_2(q(x)) \leq 0, \quad g_3(q, u(q, x)) \leq 0,$$

where $x \in X \subset R^{n_c}$ describe our CAD-Free parameterization (Mohammadi (1997a)). $q(x)$ describes all geometrical entities (normals, surfaces,...). $u \in R^N$ denotes the state variables (here the potential, electric field, fluid velocity, and the advected species) and $E \in R^N$ the state equations described above. g_1 defines the constraints expressed directly on the parameterization and is taken into account in the definition of the admissible space X, g_2 defines constraints on geometrical quantities (for instance concerning the regularity of the shape) and g_3 state constraints on u (for instance concerning the regularity of the velocity field).

3.1. *Robustness*

In many microfabricated fluidic channel systems (Molho *et al.* (2000)), it is difficult to exactly realize proposed shapes due to small but significant errors introduced in the manufacturing step. One way to account for these variations is to introduce a random perturbation operator in the optimization algorithm in the sense that the proposed shape is equivalent to any shapes in a given range (e.g. 5% in normal variation). The minimization problem (3.1) can therefore be reformulated as:

$$\min_{x(t)\in X} \max_{y\in Y(X)} J(y, q(y), u(q, y)), \tag{3.2}$$

with the state equation and constraints as above. Here the admissible space $Y(X)$ for the worst case analysis approach is defined by:

$$Y(X) = \{y \in [\frac{1}{\alpha}x, \alpha x], \forall x \in X\} \subset R^{n_c},$$

which, for instance, for $\alpha = 1.05$ defines a 5% variation range around the proposed shape. If $\alpha = 1$, there is no randomness and the two optimization problems (3.1-3.2) are similar.

Another way to proceed is to perform the optimization in an admissible space with slightly less regularity required than what would be realizable by the manufacturing. Hence, the obtained shapes includes a possible imperfection. We propose the following approach:

- Define the admissible space X for the manufacturing,
- Extend X to X' including less regular shapes,
- Perform the optimization (3.1) in X',
- Project the optimized shape into X,
- Validate the regularized shape for the skew.

This approach is easy to account for in our CAD-Free parameterization presented bellow. We show in (Fig. 1) a possible loss of regularity for the shape; three designs have been performed under the same conditions but with slightly different minimum required regularity for the admissible spaces.

4. CAD-Free shape and mesh deformation tools

The shape deformation is done in a CAD-Free framework (Mohammmadi & Pironneau (2000)) in the sense that the only entity known during optimization is the mesh. This parameterization has several characteristics:

1. All of the nodes on the inner wall of the channel are control points. More precisely, we use the local normal to the inner channel wall and specify the deformations in the direction of this normal $n(x)$. Hence, for a curve $\gamma(x)$, a deformation of amount $f(x)$, defined for each node, leading to the deformed curve $\tilde{\gamma}(x)$, can be expressed in the normal direction to γ by:

$$\tilde{\gamma}(x) = \gamma(x) + f(x)n(\gamma(x)).$$

2. To avoid oscillations, a 'local' smoothing operator is defined over the shape.

The smoothing operator is required because the gradient has less regularity than the parameterization. Indeed, suppose that the cost function is a quadratic function of the parameterization: $J(x) = (Ax - b)^2$ with $x \in H^1(\Gamma)$, $A \in H^{-1}(\Gamma)$ and $b \in L^2(\Gamma)$. The gradient $J'_x = (2(Ax-b)A) \in V$ with $H^{-1}(\Gamma) \subset V \subset L^2(\Gamma)$. Hence, any parameterization variation using J'_x as descent direction will have less regularity than x: $\delta x = -\rho J'_x =$

$-\rho(2(Ax-b)A) \in V$, where $H^{-1}(\Omega) \subset V \subset L^2(\Omega)$. We need therefore to project into $H^1(\Omega)$ using the localized solution of a second order elliptic system in regions where the deformation is not smooth enough.

$$(I - \varepsilon\Delta)\delta\tilde{x} = \delta x, \tag{4.1}$$

$$\delta\tilde{x} = \delta x = 0 \quad \text{where constrained,}$$

where $\delta\tilde{x}$ is the smoothed shape variation for the shape nodes and δx is the variation given by the optimization tool. By 'local' we mean that if the predicted shape is locally smooth, it remains unchanged during this step and ε is set to zero for these regions if,

$$\frac{\delta_{ij}(\delta x)}{(\delta x)_T} < TOL, \tag{4.2}$$

where $\delta_{ij}(\delta x)$ is the difference between the variations of the two nodes of each boundary edge and $(\delta x)_T$ the mean variation on this edge and TOL a regularity tolerance factor.

To include a loss of regularity as discussed above, it is sufficient to ask for more tolerance in the step above.

Once the shape deformation is defined, it is propagated over the computational domain using an elasticity based procedure as described in (Mohammmadi & Pironneau (2000)). These shape and mesh deformation tools have been used in optimization problems in two- and three-dimensional configurations for incompressible and compressible flows (Mohammmadi & Pironneau (2000)).

5. Cost function and constraints

We want to minimize the skew, which can be quantified in different ways. For example, we can ask for iso-values of the advected species to be always normal to the flow field. In this case, we can consider:

$$J(x) = \int_0^T \int_\Omega (\nabla a(x,t) \times U(x))^2 dx dt, \tag{5.1}$$

where T is the maximum migration time. These integrals are not suitable for cheap sensitivity evaluation as they involve information over the whole domain. In addition, this cost function is too restrictive as we are actually interested only in minimizing the final skew. The cost function reduces to:

$$J(x) = \int_\Omega (\nabla a(x,T) \times U(x))^2 dx, \tag{5.2}$$

which again reduces away from the turn, and therefore where U is constant, to:

$$J(x) = \int_\Omega (\frac{\partial a(x,T)}{\partial n})^2 dx, \tag{5.3}$$

where n is the normal direction to the local walls.

Another way to reduce the skew, which avoids the previous restriction, is to ask for all particles traveling on characteristics to have the same migration time. Hence, the cost function is given by:

$$J(x) = (\int_\chi \frac{ds}{U} - \int_{\chi'} \frac{ds}{U})^2, \tag{5.4}$$

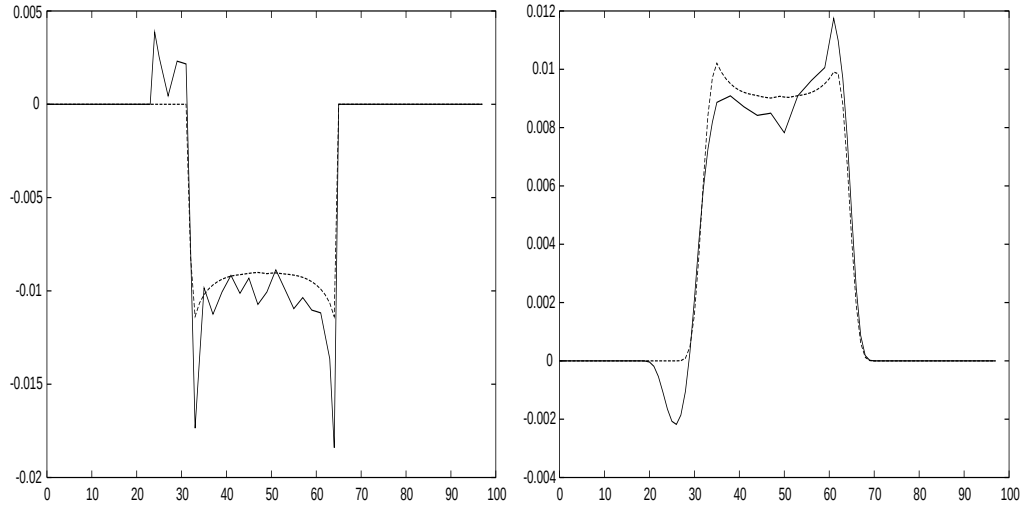

FIGURE 2. Sensitivity evaluation around the initial 90-degree turn for control points along the inner channel wall. Comparison between the exact (———) and incomplete (- - - -) gradient evaluations (left). The deformations obtained using these gradients (right).

for any couple of characteristics χ and χ' linking the outlet to the inlet. Here again, the cost function is over the whole space, but we can consider only a few characteristics. The two main characteristics are those defined by the internal and external walls of the channel:

$$J(x) = (\int_{\Gamma_i} \frac{ds}{U.\tau} - \int_{\Gamma_o} \frac{ds}{U.\tau})^2. \tag{5.5}$$

where Γ_i is the inner wall and Γ_o the outer wall in a turn. This last formulation is interesting as it only involves boundaries which we know to be suitable for the application of our incomplete sensitivity. Another interesting feature of formulations (5.4 and 5.5) over (5.1) is that they do not require the knowledge of the distribution of the advected species.

As we said, we notice that the residual band advection dispersion away from the channel walls increases with the variation of the shape curvature. We therefore add the following constraint to the cost function (5.5) above:

$$J(x) \leftarrow J(x) + (\int_{\Gamma_i} \|\frac{\partial n}{\partial s}\| - \int_{\Gamma_i^0} \|\frac{\partial n}{\partial s}\|)^2 + (\int_{\Gamma_o} \|\frac{\partial n}{\partial s}\| - \int_{\Gamma_o^0} \|\frac{\partial n}{\partial s}\|)^2, \tag{5.6}$$

where 0 denotes initial inner and outer walls. Thus, when we allow both walls to move, we obtain about the same amount of skew but a higher residual dispersion inside the channel. The second constraint vanishes in cases where the outer wall is kept unchanged.

Two other types of geometrical constraints concern the amplitude of the deformations and the regularity of the deformed shape. In the first constraint, shape variations are allowed between two limiting curves. Regularity requirements are enforced using the smoothing operator of the CAD-Free parameterization described above.

6. Sensitivity and incomplete sensitivities

Consider the general simulation loop, involved in (3.1), leading from shape parameterization to the cost function:

$$J(x) : x \to q(x) \to U(q(x)) \to J(x, q(x), U(q(x))).$$

The Jacobian of J is given by:

$$\frac{dJ}{dx} = \frac{\partial J}{\partial x} + \frac{\partial J}{\partial q}\frac{\partial q}{\partial x} + \frac{\partial J}{\partial U}\frac{\partial U}{\partial q}\frac{\partial q}{\partial x}.$$

In most applications, the cost function is, or can be reformulated to have, the following characteristics:

- The cost function J and the parameterization x are defined on the shape (or some part of it),
- J is of the form

$$J(x) = \int_{\text{shape or part of the shape}} f(x, q)g(u)d\gamma,$$

which means that it involves a product of geometrical and state based functions.

We have shown that for such cost functions, the sensitivity with respect to the state can be neglected in regions where the curvature of the shape is not too large (Mohammadi (1997a)-Mohammadi (1999)).

The concept of incomplete sensitivities was first introduced for aerodynamical applications involving hyperbolic and parabolic PDEs (Mohammmadi & Pironneau (2000)). In that work, we showed that where the cost function, constraints, and controls are defined over the shape (through boundary integrals for instance), a good estimation of gradients are obtained by keeping only geometrical sensitivities. This means that only the shape deformation tool has to be differentiated and not the whole simulation loop. In particular, neither the mesh deformation nor the state equation solver have to be linearized (Mohammadi (1997b)). Hence, we consider the following approximation for the gradient:

$$\frac{dJ}{dx} \sim \frac{\partial J}{\partial x} + \frac{\partial J}{\partial q}\frac{\partial q}{\partial x}.$$

We can illustrate this idea by the following simple example. Consider as cost function $J = a^n u_x(a)$ and for the state equation the following diffusion equation:

$$-u_{xx} = 1, \quad \text{on }]\epsilon, 1[, \quad u(\epsilon) = 0, \quad u(1) = 0,$$

which has as solution $u(x) = -x^2/2 + (\epsilon+1)/2 - \epsilon/2$. We are in the domain of application of the incomplete sensitivities (Mohammmadi & Pironneau (2000)):

- the cost function is product of state and geometrical quantities (larger is n, better is the approximation),
- it is defined at the boundary,
- the curvature of the boundary is small (here no curvature at all).

The gradient of J with respect to ϵ is given by:

$$J_\epsilon(\epsilon) = \epsilon^{n-1}(nu_x(\epsilon) + \epsilon u_{x\epsilon}(\epsilon)) = \frac{\epsilon^{n-1}}{2}(-n(\epsilon+1) - \epsilon).$$

The second term between parenthesis is the state linearization contribution which is neglected in incomplete sensitivities. We can see that the sign of the gradient is always correct and the approximation is better for large n.

As we stated above, the cost function (5.5) is suitable for the application of incomplete sensitivities. We can increase direct geometrical contributions because the velocity is parallel to the walls. The cost function we consider for derivation is therefore:

$$J(x) = (\int_{\Gamma_i} \frac{ds}{\vec{\tau}\mu_{ek}|E|} - \int_{\Gamma_o} \frac{ds}{\vec{\tau}\mu_{ek}|E|})^2., \tag{6.1}$$

where $\vec{\tau}$ is the local unit tangent vector to the wall.

To evaluate the accuracy of these gradients, we compare the results obtained with this approximation of the gradients with those coming from finite differences. This incomplete sensitivity evaluation shows the importance of redefining cost functions as boundary integrals when possible (as shown above) and of locating the cost function and control definition locations as close to each other as possible. This is in particular important for three-dimensional configurations and it also permits optimization of an entire microfluidic network and not only a small section of the network. In fact, optimization becomes possible for any geometry for which simulation is affordable as the cost of simulation and design becomes equivalent. Indeed, sensitivity analysis is now equivalent to the linearization of the following approximate simulation loop:

$$\tilde{J}(x) : x \to q(x)|_\Gamma \to J(x, q(x), U(q(x))),$$

which means that we only account for the modification in the geometrical part defined over the inner channel wall.

6.1. *Multi-level gradient construction*

The above discussion of incomplete sensitivities demonstrates that an accurate state evaluation and an approximate gradient is preferable over an accurate gradient based on an inaccurate state obtained from a coarse mesh.

Consider a bilinear cost function involving state u and geometrical q contribution and defined over the same region as the control x.

$$|\frac{d}{dx}(u.q) - u(\text{fine})\frac{dq}{dx}| < |\frac{d}{dx}(u.q) - \frac{du}{dx}(\text{coarse}).q + u(\text{coarse})\frac{dq}{dx}|.$$

The left-hand side is the difference between exact and incomplete gradient computed on a fine mesh.

This error is often present and is due to the fact that the cost of iterative minimization and gradient evaluations limits the user to coarser meshes than what would have been used for a pure simulation.

One method for avoiding this difficulty is to use different levels of refinement for the state and the gradient. This is the idea behind multi-level shape optimization where the gradient is only computed on the coarse level of a multi-grid construction and where the state comes from the finer level (Beux & Dervieux (1997)):

$$\frac{d}{dx}(u.q)(\text{fine level}) = I(\frac{du}{dx}(\text{coarse level})).q(\text{fine}) + u(\text{fine level})\frac{dq}{dx}(\text{fine}).$$

The first term of the left-hand side is the interpolation of the gradient computed on the coarse grid over the fine level.

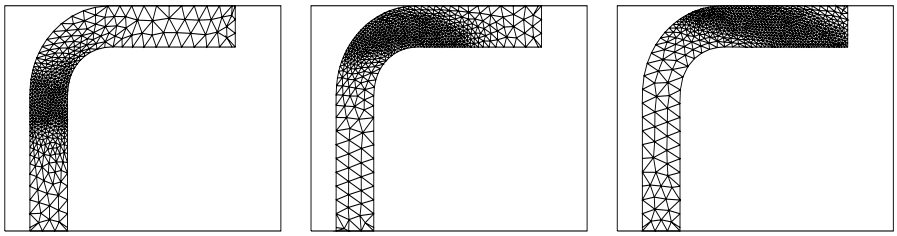

FIGURE 3. Adaptive simulation to accurately capture the skew.

7. Pseudo-unsteady closure equation for x

Consider the following time dependent equation for the shape parameterization x. Here, the time is fictitious and is similar to the descent parameter.

$$\dot{x} + \epsilon \ \ddot{x} = -F(\Pi, \mathcal{M}^{-1}, \nabla_x J).$$

F is a function of the exact or incomplete gradient; it accounts for the projection over the admissible space and the smoothing operator $(\Pi, \mathcal{M})$. This system represents most minimization algorithms. If $\epsilon = 0$, we recover the steepest descent approach. If $\epsilon > 0$, this is the heavy ball method (Attouch & Cominetti (1996)) The aim in this approach is to access different minima of the problem and not only the nearest local minimum. Conjugate gradient and quasi-Newton methods can also be cast in this form (Mohammmadi & Pironneau (2000)).

To advance in time (7), we use a central difference scheme (denoted by δx^p, the shape deformation at step p):

$$(\frac{\epsilon}{\lambda^2} + \frac{1}{\lambda})\delta x^{p+1} = \frac{\epsilon}{\lambda^2}\delta x^p - F(\nabla_{x^p} J^p). \tag{7.1}$$

After defining the shape parameterization, x^0, the dynamical algorithm we use is as follows:

Optimization iterations

1. compute the gradient: $\frac{dJ^p}{dx}$ or $\frac{d\tilde{J}^p}{dx}$,
if $(\|\frac{d\tilde{J}^p}{dx}\| < TOL$ or $J^p < TOL)$ stop.
2. define the new admissible shape deformation using (7.1): δx^p,
3. smooth the deformations using (4.1),
4. deform the mesh.
5. compute the new state: u^{p+1}.
6. compute the new cost: J^{p+1}.
7. $p \leftarrow p + 1$ and goto 1.

End of optimization loop.

8. Numerical results

In addition to the characteristics presented above, we use a Delaunay mesh adaptation technique by local metric control that is widely used in various simulations involving the solution of PDE's (Frey & George (1999), Hecht & Mohammadi (2000)). The impact of this coupling has been shown on the advection of a passive scalar by the electric field (Fig. 3). It is clear that to have the same quality without mesh adaptation implies the

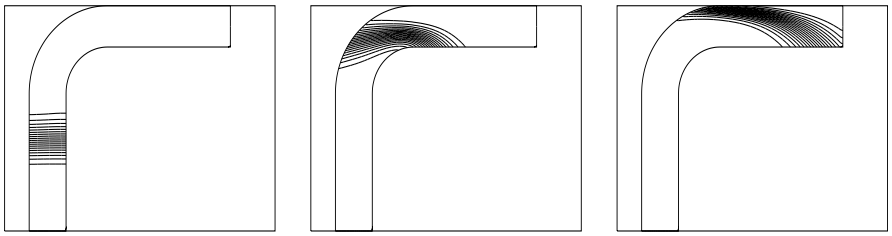

FIGURE 4. Initial shape for the 90-degree turn: effect of the turn on the advected species.

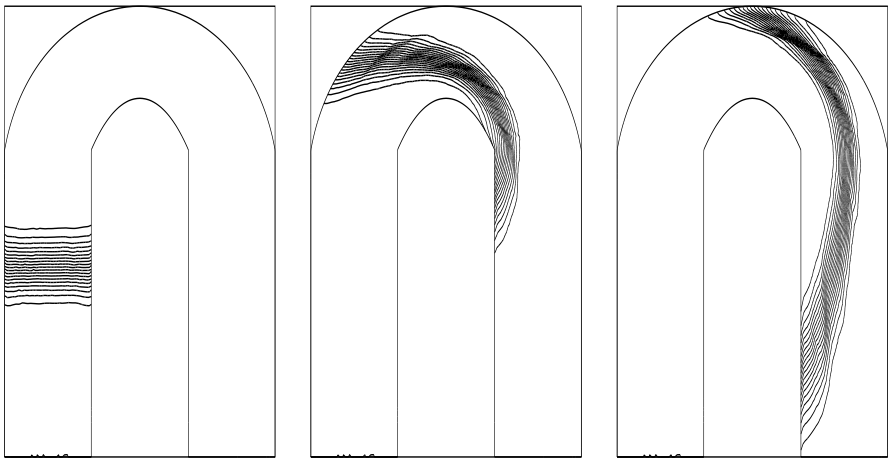

FIGURE 5. Initial shape for the 180-degree turn: effect of the turn on the advected species.

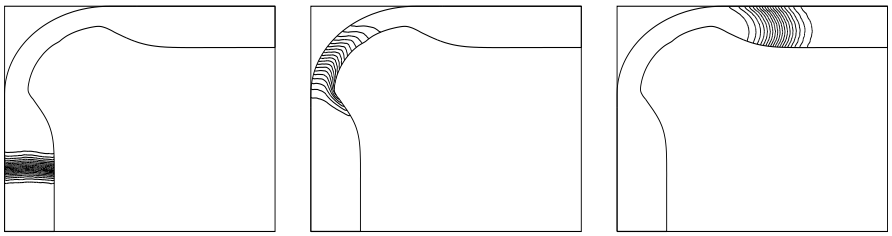

FIGURE 6. First class of optimized shapes for the 90-degree turn. The magnitude of the skew has been reduced by one order.

use of a regular fine mesh everywhere, which is out of reach for general applications. The remeshing is also important and absolutely necessary as the large deformations introduced for the shape makes the mesh too distorted to be effective for finite element simulations.

We show the skews produced by 90- and 180-degree turns in Figs. (4-5). We then applied our optimization approach to these configurations. No symmetry assumption has been made. The first class of optimized shapes for the 90- and 180-degree turns (Figs. 6-7) correspond well with what was found by an intuitive design (Molho *et al.* (2000)). This is important as it permits some confidence on the global design approach. The second classes of optimized shapes for the 90- and 180-degree turns (Figs. 8-9) have been obtained by

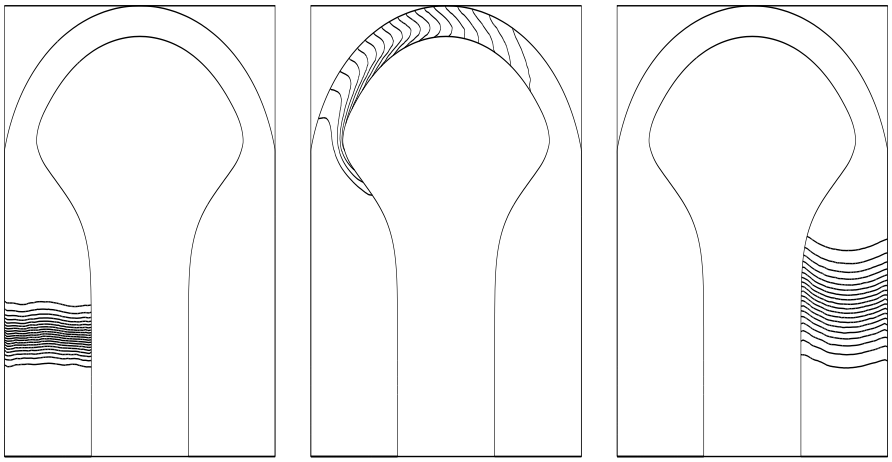

FIGURE 7. First class of optimized shapes for the 180-degree turn. The magnitude of the skew has been reduced by more than one order.

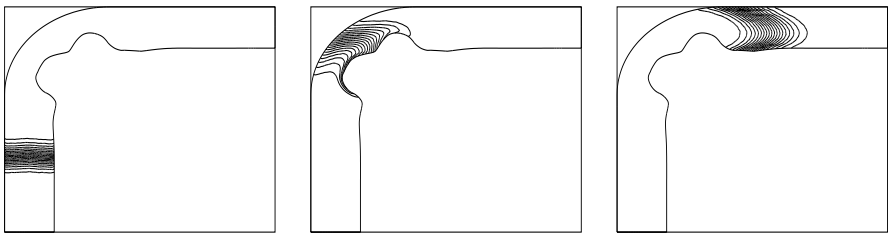

FIGURE 8. Second class of optimized shapes for the 90-degree turn. The magnitude of the skew is about the same than for the first class above with 15% less reduction in cross-section, but there is more dispersion in the advection band as the wall curvature variation is higher.

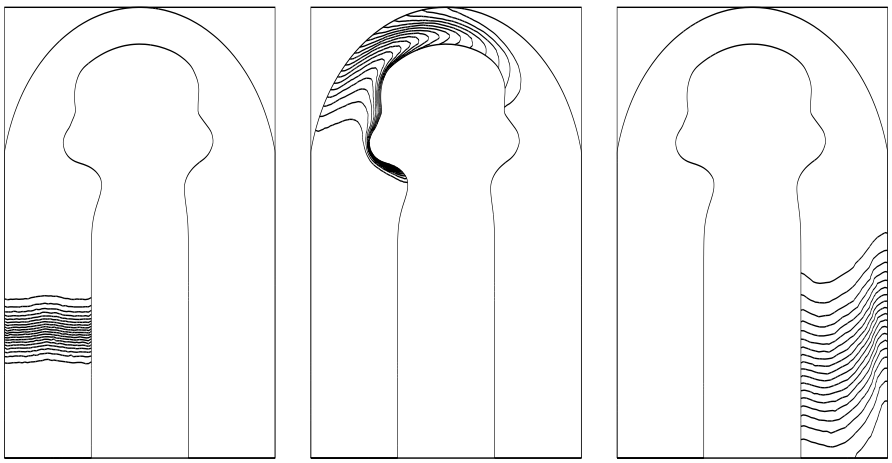

FIGURE 9. Second class of optimized shapes for the 180-degree turn. Here again, larger curvature variation introduces more dispersion in the advection band away from walls.

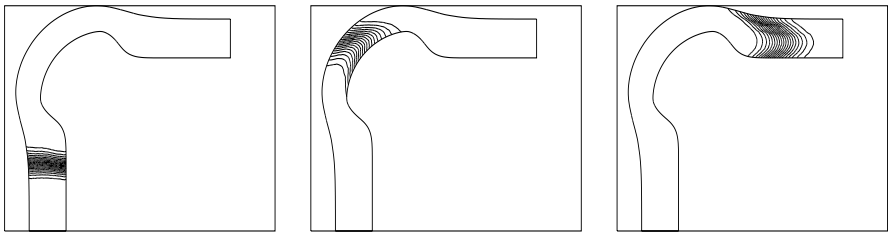

FIGURE 10. Third class of optimized shapes for the 90-degree turn with both the inner and outer walls modified. The skew is about the same than for the first class of the 90-degree optimized turn but with a much larger cross-section, but also more band dispersion away from walls.

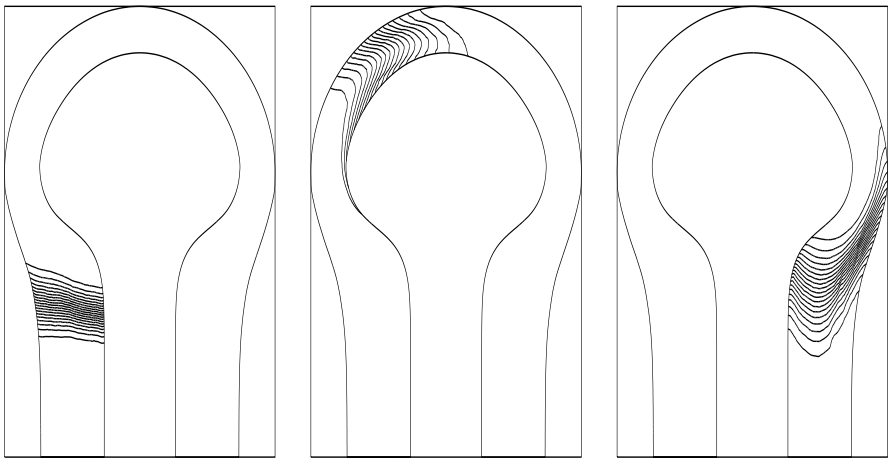

FIGURE 11. Third class of optimized shapes for the 180-degree turn with both the inner and outer walls moving. The skew has been quite reduced and the cross-section conserved (compared to the first class of shape), but there is much more band dispersion away from walls.

constraining the reduction in cross-sectional area and by requiring less regularity for the shapes. However, the increase in irregularity leads to more band dispersion away from the channel walls. The optimizations described above were performed without altering the shape of the outer wall. To avoid too much restriction in the channel cross-section, a third class of shape can be obtained by allowing both the inner and outer walls to deform (Figs. 10-11). However, this turn is less interesting as two such turns would interfere when used to create a serpentine channel pattern.

9. Concluding remarks

We have shown how to combine incomplete sensitivity analysis and the pseudo-unsteady optimization approach to design reduced dispersion electrokinetic microchannel devices. This analysis implies a redefinition of the cost function used for sensitivity evaluation based on approximate formula through boundary integrals. In addition, it has been shown that, to reduce the dispersion associated with band advection away from the channel walls, these walls need to be smooth with minimal curvature variation along the walls. Using the ingredients presented in this paper, minimal dispersion 90- and 180-

degree turns have been obtained which enable, by their combination, the construction of long microfluidic channels within a compact area.

Acknowledgments

This work has been partly supported by the Center for Turbulence Research at Stanford University. Many thanks to Profs. P. Moin, B. Perthame, and O. Pironneau for their interests in this work. Many thanks to D. Spinks and M. Fatica for their assistance during the summer institute.

REFERENCES

Culbeston, C. T., Jacobson, S. C. & Ramsey, J. M. 1998 Dispersion Sources for Compact Geometries on Microchips. *Analytical Chemistry.* **70**, 3781-3789.

Molho, J. I., Herr, A. E., Mosier, B. P., Santiago, J. G., Kenny, T. W., Brennen, R. A. & Gordon, G. B. 2000 Designing Corner Compensation for Electrophoresis in Compact Geometries. *Proc. Micro Total Analysis Systems 2000.*

Mohammadi, B. 1997 Practical Applications to Fluid Flows of Automatic Differentiation for Design Problems. *VKI lecture series, 1997-05.*

Mohammadi, B. 1997 A New Optimal Shape Design Procedure for Inviscid and Viscous Turbulent Flows. *Int. J. for Num. Meth. in Fluid.* **25**, 183-203.

Mohammadi, B. & Pironneau, O. 2000 *Applied Shape Design for Fluids*, Oxford Univ. Press.

Mohammadi, B. 1999 Flow Control and Shape Optimization in Aeroelastic Configurations. *AIAA 99-0182.*

Probstein, R. F. 1995 *Physicochemical Hydrodynamics*, Wiley.

Beux, F. & Dervieux, A. 1997 A Hierarchical approach for shape optimisation. *Inria report 1868.*

Attouch, H., Cominetti, R. 1996 A Dynamical Approach to Convex Minimization Coupling Approximation with the Steepest Descent Method. J. Diff. Eq. **128**(2), 519-540.

Frey, P. & George, P. L. 1999 *Maillages*, Hermes.

Hecht, F. & Mohammadi, B. 2000 Mesh Adaptation for Time Dependent Simulation and Optimization, *Revue Europèenne des Elements Finis,* submitted.